ACS OMEGA

Open Access

http://pubs.acs.org/journal/acsodf

Article

Size-Dependent Cytotoxicity, Adhesion, and Endocytosis of Micro-/Nano-hydroxyapatite Crystals in HK-2 Cells

Jin Han, Xin-Yi Tong, Chen-Ying Rao, Jian-Ming Ouyang,* and Bao-Song Gui*

Cite This: *ACS Omega* 2023, 8, 48432−48443

Read Online

ACCESS | Metrics & More | Article Recommendations

ABSTRACT: Nano-hydroxyapatite (nano-HAP) is often used as a crystal nest to induce calcium oxalate (CaOx) kidney stone formation, but the mechanism of interaction between HAP crystals of different properties and renal tubular epithelial cells remains unclear. In this study, the adhesion and endocytosis of HAP crystals with sizes of 40 nm, 70 nm, 1 μm, and 2 μm (HAP-40 nm, HAP-70 nm, HAP-1 μm, and HAP-2 μm, respectively) to human renal proximal tubular epithelial cells (HK-2) were comparatively studied. The results showed that HAP crystals of all sizes promoted the expression of osteopontin and hyaluronic acid on the cell surface, destroyed the integrity of the lysosomes, and induced the apoptosis and necrosis of cells. Nano-HAP crystals had a higher specific surface area, a smaller contact angle, a higher surface energy, and a lower Zeta potential than those of micro-HAP. Therefore, the abilities of HK-2 cells to adhere to and endocytose nano-HAP crystals were greater than their abilities to do the same for micro-HAP crystals. The order of the endocytosed crystals was as follows: HAP-40 nm > HAP-70 nm > HAP-1 μm > HAP-2 μm. The endocytosed HAP crystals entered the lysosomes. The more crystal endocytosis and adhesion there is, the more toxic it is to HK-2 cells. The results of this study showed that nanosized HAP crystals greatly promoted the formation of kidney stones than micrometer-sized HAP crystals.

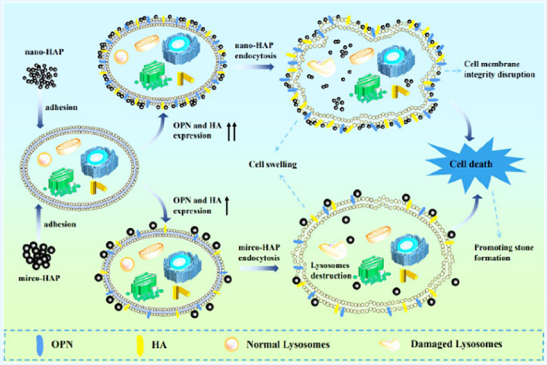

1. INTRODUCTION

The formation of calcium oxalate (CaOx) kidney stones is related to the deposition of calcium phosphate on the renal papillae.[1,2] Various calcium phosphate salts, such as calcium phosphate (CaP), amorphous calcium phosphate, and hydroxyapatite (HAP), are present in urine.[3−5] These salts can be used as crystal nests to induce the formation of CaOx stones.[6,7]

The formation of kidney stones is also closely related to oxidative damage to renal epithelial cells.[8,9] Calcium phosphate precipitation can cause damage to renal tubular cells, leading to the expression of distal tubule-associated adhesion proteins such as osteopontin (OPN) and hyaluronic acid (HA). These molecules promote the adhesion of calcium phosphate to the surface of renal tubular cells.[10] As calcium phosphate deposits grow and expand into the interstitial space and become embedded in the matrix, Randall plaques form and extend to the basal side of the urothelium, leading to pathological renal calcification.[4]

CaOx kidney stones have been widely explored. CaOx crystals can adhere to renal tubular epithelial cells and deposit in the renal tubular lumen and renal interstitium, causing damage to renal tissues and impairing their functions.[11] The adhesive effect of crystals and cells is an early process of kidney stone formation. The adhered crystals can be further endocytosed by cells. A small degree of endocytosis is helpful for reducing the number of adhesion sites on a cell surface, but an excessive degree of endocytosis may exacerbate cell damage.[12] However, few reports on the effect of HAP adhesion and endocytosis on renal epithelial cells have been presented.

The size and morphological characteristics of HAP affect its cytotoxicity. Shi et al.[13] studied the adhesion and endocytosis of rod-shaped HAPs of different sizes (20 nm, 80 nm, and 12 μm) in human umbilical vein endothelial cells and the effects of these crystals on cell function. They observed that HAP can accumulate in the cytoplasm, and nano-HAP crystals adhere to the cells in a maximum of 180 min; furthermore, their endocytosis reaches the maximum at 45 min. The adhesion and endocytosis of micro-HAP crystals are significantly lower than those of nano-HAP crystals and remain almost constant over time. Therefore, nano-HAP crystals more easily adhere to and become endocytosed by cells than micro-HAP crystals do. As

Received: October 18, 2023
Revised: November 19, 2023
Accepted: November 24, 2023
Published: December 5, 2023

Table 1. Basic Physical and Chemical Properties of HAP with Different Sizes

crystal type	crystal size[a]	specific surface area $S_{BET}/m^2/g$	zeta potential in culture/mV	cell viability[b]/%
HAP-40 nm	37.9 ± 8.7 nm	76.2	−3.21	64.3
HAP-70 nm	71.3 ± 5.4 nm	67.0	−4.14	69.1
HAP-1 μm	1.0 ± 0.2 μm	6.16	−13.94	81.5
HAP-2 μm	1.9 ± 0.6 μm	1.18	−24.08	89.1

[a]The average crystal size was determined by Nano Measurer 1.2.5 Software from the SEM images. [b]Cell viability after 24 h of injury at a crystal concentration of 250 μg/mL.

such, the cell damage caused by the former is more serious than that induced by the latter.

The cytotoxicity of HAP is closely related to its size and morphological characteristics.[9] The cytotoxicity of HAP crystals with different morphological characteristics is positively related to the following factors of crystals: large specific surface area, sharp edges, large aspect ratio, and small absolute Zeta potential. However, differences in the adhesion and endocytosis of HAP crystals with different sizes in renal epithelial cells have not been reported.

In this study, differences in the adhesion and endocytosis of HAP crystals with sizes of 40 nm, 70 nm, 1 μm, and 2 μm in human renal proximal tubular epithelial cells (HK-2) were comparatively examined to further understand the effect and mechanism of HAP crystal size and Randall plaque on the formation of CaOx kidney stones.

2. EXPERIMENTAL METHODS

2.1. Materials and Apparatus. *2.1.1. Material.* HAP crystals with sizes of 37.9 ± 8.7 nm, 71.3 ± 5.4 nm, 1.0 ± 0.2 μm, and 1.9 ± 0.6 μm (named HAP-40 nm, HAP-70 nm, HAP-1 μm, and HAP-2 μm, respectively) were purchased from Huizhou Weijing New Material Co., Ltd., its basic physical and chemical properties are shown in Table 1, and SEM images are shown in Figure 1.

HK-2 was obtained from Shanghai cell bank of the Chinese Academy of Sciences; DMEM/F12 medium, fetal bovine serum, penicillin, and streptomycin were purchased from Gibco Biochemicals (Beijing) Co., Ltd.; 6, 12, and 96-well cell culture plates were purchased from NEST, Nice Biotechnology (Wuxi) Co., Ltd.; fluorescein isothiocyanate (FITC) was purchased from Shanghai Aladdin Biochemical Technology Co., Ltd.; OPN antibody, FITC-labeled goat antirabbit IgG antibody, DiI (cell membrane red fluorescent probe), 4,6-diamino-2-phenylindole (DAPI) staining solution, and bHABP were purchased from Shanghai Biyuntian Biotechnology Co., Ltd.. Other conventional chemical reagents are analytically pure and were purchased from Guangzhou Chemical Reagent Factory.

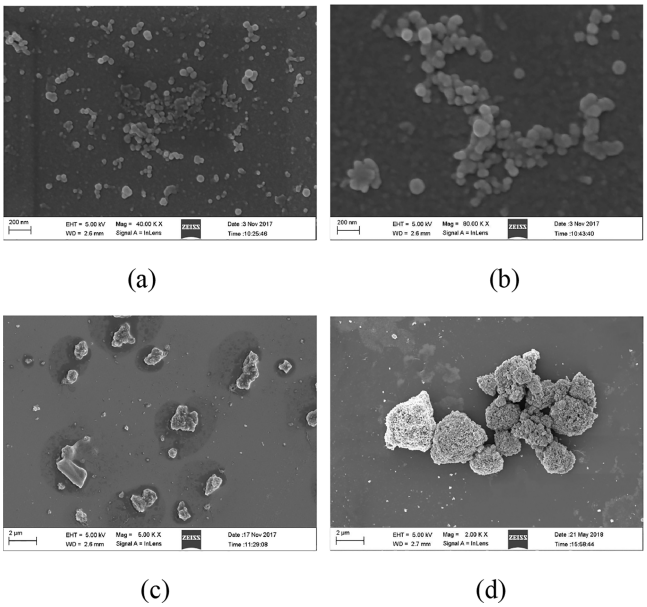

Figure 1. SEM images of different sizes of HAP crystals: (a) HAP-40 nm, (b) HAP-70 nm, (c) HAP-1 μm, and (d) HAP-2 μm.

2.1.2. Apparatus. Contact angle measuring instrument (Kruss, Germany); optical microscope (Olympus, CKX41, Japan); confocal microscope (LSM510 Meta Duo Scan, Zeiss, Jena, Germany); flow cytometer (Beckman, Gallios, (USA); X-L type environmental scanning electron microscope (SEM, Philips, Eindhoven, Netherlands); and inverted fluorescence microscope (IX51, Olympus, Tokyo, Japan).

2.2. Contact Angle Detection of Different Sizes of HAP. The surface wettability of the material was evaluated by measuring the contact angle between the HAP crystals and the water droplets. 1 mg of HAP crystals was taken for tableting, 2 drops of distilled water was dropped on the sample, and the contact angle was measured at room temperature.

2.3. Cell Culture and Grouping. Preparation of the HAP crystal suspension: a certain amount of HAP crystals was flattened, sterilized by UV for 30 min, and then dispersed in serum-free culture solution, formulated into a suspension with a concentration of 250 μg/mL for use, and ultrasonicated for 5 min before use.

HK-2 cells were cultured in DMEM/F12 medium containing 10% fetal bovine serum at 37 °C, 5% CO_2, and saturated humidity. Cells were passaged using the trypsin digestion method. After the cells were synchronized, the cells were divided into 2 groups: (A) control group: only serum-free culture solution was added; (B) crystal treatment group: HAP-40 nm, HAP-70 nm, HAP-1 μm, or HAP-2 μm crystals with a concentration of 250 μg/mL were added, respectively.The cells in each group were incubated for 24 h.

2.4. Qualitative and Quantitative Detection of OPN Expression. Experimental grouping was the same as that in Section 2.3. After the cells were fixed with 4% paraformaldehyde for 10 min, the sheep serum was added to incubate the cells for 20 min. The first antibody of the OPN was dropped into the samples (1:100) and incubated at 4 °C overnight. Afterward, the FITC secondary antibody (1:100) was added dropwise in the dark. After incubation at 37 °C for 30 min, the cells were stained and sealed with DAPI. The expression of the OPN was observed using a laser confocal microscope.

Quantitative detection of OPN expression: referring to the above method, a 96-well plate was used to quantitatively detect the fluorescence intensity by a multifunctional microplate reader.

https://doi.org/10.1021/acsomega.3c08180
ACS Omega 2023, 8, 48432−48443

2.5. Qualitative and Quantitative Detection of HA Expression. Experimental grouping was the same as those in Section 2.3. Cells were fixed with a fixative solution (composed of 5% glacial acetic acid, 10% formalin, and 70% alcohol) for 20 min. After washing the cells 3 times, 100 μL of 5 μg/mL bHABP solution (prepared in 3% bovine serum albumin) was added and incubated at 4 °C overnight. Then, 100 μL of FITC-avidin was added to these samples, and the mixture was incubated for 1h. After that, DAPI staining solution was added to counterstain for 4 min. Finally, the cells were sealed with an antiquenching agent. The HA expression (green fluorescence) was observed using a confocal microscope.

Quantitative analysis of the HA green fluorescence intensity: the Axiovision software (ZEISS, Germany) attached to the instrument was used to detect 100 cells and averaged.

2.6. Lysosomal Integrity Detection. Qualitative analysis: experimental grouping were the same as those in Section 2.3. 1 mL of cell suspension with a cell concentration of 1×10^5 cells/mL was inoculated per well in 12-well plates. Five μg/mL (prepared by DMEM) acridine orange was added to stain the cells for 15 min. After treatment, the distribution of acridine orange in cells was observed by a fluorescence microscope.

Quantitative analysis: 100 μL of cell suspension with a cell concentration of 1×10^5 cells/mL was inoculated per well in 96-well plates. After the same treatment as above, Enzyme mark instrument was used to detect the red and green fluorescence intensity. The excitation wavelength is 485 nm, and the reflection wavelength is 530 nm (green cytoplasmic AO) and 620 nm (red lysosomal AO). Control group lysosomal integrity = red light intensity/green light intensity. HAP treatment group lysosomal integrity = red light intensity/(green light intensity × control lysosomal integrity).

2.7. Apoptosis and Necrosis Detection. Experimental grouping was the same as those in Section 2.3. 800 μL of cell staining buffer, 5 μL of Hoechst staining solution, and 5 μL of PI staining solution were added into the cells. The sample was mixed thoroughly and incubated at 4 °C for 25 min. The cells were observed by a fluorescent microscope. Hoechst 33342 shows blue fluorescence, and PI shows red fluorescence.

2.8. Detection of Different Size HAP Adhesion on the HK-2 Cell Surface. Qualitative microscopic examination: experimental grouping were the same as those in Section 2.3, each group was incubated at 4 °C for 1 h to inhibit the cell endocytosis activity.[14] After aspirating the supernatant, the cells were washed 5 times with cold PBS to remove unadhered and tightly unadherent crystals. 2.5% glutaraldehyde was added to fix for 24 h, and then the cells were dehydrated by gradient ethanol (30, 50, 70, 90, and 100%). The sample was observed under microscope after CO_2 drying.

Quantitative detection by flow cytometry[15]: FITC-labeled HAP crystals, experimental grouping was the same as those in Section 2.3. The cells of each group were transferred to 4 °C and incubated for 1 h. After aspirating the culture fluid, the cells were washed with cold PBS to remove unadhered and tightly unadherent crystals. The cells were resuspended with PBS after trypsin digestion. The flow cytometry was used for detection. The cells with the FITC signal were regarded as the cells with adherent crystals.

2.9. Detection of HK-2 Cells Endocytoses HAP by Flow Cytometry. After incubating the nano-HAP crystals with the cells for 24 h, the supernatant was aspirated and the adherent crystals on the cell surface were removed by complexation with 5 mM EDTA for 5 min[16] and washed twice with PBS. The cells were collected by trypsin digestion, followed by centrifugation (1000 rpm/min). The supernatant was removed, and the cells were washed with PBS and resuspended. After treatment, the samples were tested on the machine. Flow cytometry was used to detect the proportion of cells endocytosing crystals. The cells with the FITC fluorescence signal can be regarded as the cells with endocytic crystals.

2.10. Distribution of Different Sizes of HAP Inside and Outside the Cell Membrane. Experimental grouping was the same as those in Section 2.3. After FITC-labeled HAP crystals (green fluorescence) and cells were incubated for 24 h, 300 μL of DiI was added to stain for 40 min to label the cell membranes (red fluorescence). Then, 4% paraformaldehyde was added to the solution and fixed for 10 min. The nuclei were stained and labeled with DAPI (blue fluorescence). The distribution of HAP crystals inside and outside the cell membrane was observed by a confocal microscope.

2.11. Wound Healing Assay. Experimental grouping was the same as those in Section 2.3. When the cells converged into a single-layer state, a linear trace with a width of about 400 μm was drawn in a certain direction with a sterile 10 μL pipet tip. Optical microscopy was used to take pictures. After washing twice with PBS, fresh medium was added to continue culturing for 48h, and the cells on the edge of the scratch would gradually enter the blank area to heal the "scratch". Finally, we took photos at the same location and calculated the healing rate of the cells.

2.12. Statistical Analysis. Experimental data were expressed as mean ± SD from at least three independent experiments. The experimental results were statistically analyzed using SPSS 13.0 software, and the Tukey test was used to analyze the differences between the means of each experimental group and the control group. $P < 0.05$ was considered statistically significant, indicating a significant difference, $P < 0.01$ indicating a very significant difference, $P > 0.05$ indicates no significant difference.

3. RESULTS

3.1. Small HAP Size Corresponds to a Small Contact Angle. Contact angle (θ) is an important property of biological coating surfaces and is implicated in the adhesion of cells and materials.[17] When $\theta < 90°$, liquids can wet crystals, and the smaller the value of θ is, the better the wettability will be. When $\theta = 0$, complete wetting occurs. When $90° < \theta < 180°$, which is also known as the hydrophobic contact angle, liquids do not wet solids. A low θ indicates a high surface energy, which is conducive to cell adhesion and growth.[15]

The four sizes of HAP crystals, namely, HAP-40 nm, HAP-70 nm, HAP-1 μm, and HAP-2 μm (Figure 1), had θ values of 21.48°, 34.21°, 38.63°, and 52.36°, respectively, which are less than 90° (Figure 2). The result indicated that they could adhere to cells, and the adhesion tendency of nano-HAP crystals is greater than that of micro-HAP crystals.

3.2. HAP Increases the Expression of OPN on the Surface of HK-2. OPN is an important adhesion molecule on cell surfaces. Cell damage causing apoptosis or necrosis can promote the OPN expression.[5] Confocal laser scanning microscopy showed that the OPN expression of HK-2 cells was caused by four HAPs (Figure 3).

Only weak green fluorescence appeared in the cells of the control group, indicating that only a small amount of OPN was expressed. However, the green fluorescence of the cells cocultured with HAP crystals was obviously enhanced, indicating that the expression of OPN increased. Meanwhile,

https://doi.org/10.1021/acsomega.3c08180
ACS Omega 2023, 8, 48432−48443

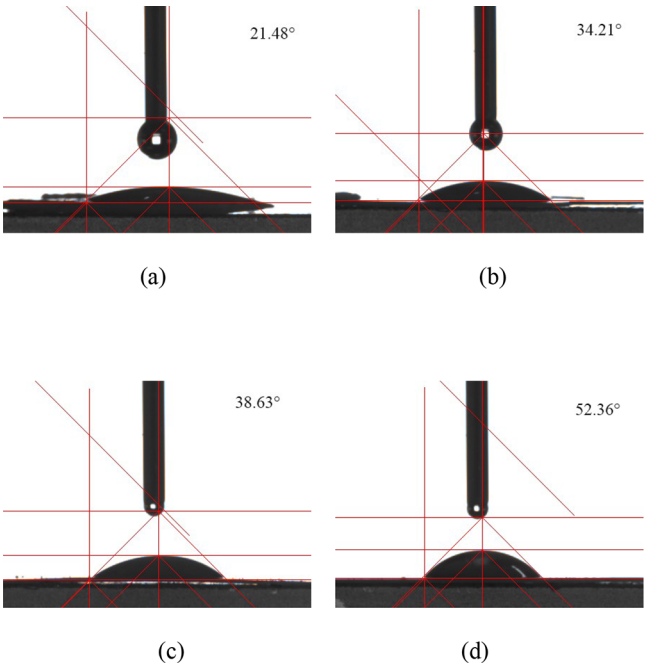

Figure 2. Contact angles of different sizes of HAP crystals: (a) HAP-40 nm, (b) HAP-70 nm, (c) HAP-1 μm, and (d) HAP-2 μm.

the degree of cell damage induced by nano-HAP was greater than that caused by micro-HAP. As a result, the OPN expression increased, and their order was: HAP-40 nm > HAP-70 nm > HAP-1 μm > HAP-2 μm (Figure 3B).

3.3. HAP Increases the Expression of HA on the Surface of HK-2. HA is another crystal adhesion molecule expressed after a cell is damaged.[18] The expression level of HA can indirectly reflect the damage of cells. Figure 4 illustrates the HA expression of HK-2 cells caused by four sizes of HAP. The green fluorescence intensity of the crystal group was stronger than that of the control group. This result suggested that HAP caused an increase in the HA expression of the cells, and the nanotreated group was stronger than the microtreated group (Figure 4B).

3.4. HAP Reduces the Lysosomal Integrity of HK-2 Cells. Acridine orange (AO) can enter lysosomes through the cell membrane structure and bind to its internal acid hydrolase to fluoresce red, whereas AO fluoresces green in the cytoplasm.[19] The smaller the amount of red fluorescence, the more severe the degree of lysosomal damage and the higher the degree of cell necrosis.[20]

The damage caused by nano-HAP crystals and micro-HAP crystals to HK-2 cell lysosomes was qualitatively analyzed through fluorescence microscopy (Figure 5A) and quantitatively detected with a microplate reader (Figure 5B). The lysosomes (i.e., orange-red fluorescence) of the control group were clearly visible. After the treatment with two nano-HAP crystals, most of the orange-red fluorescence disappeared and the green fluorescence remained in the cells, indicating that the lysosomal integrity of the cells was severely damaged. By contrast, the effect of two micro-HAPs on lysosomal integrity was less than that of nano-HAPs. The results of the quantitative analysis of the degree of damage induced by the four crystals on the integrity of lysosomes are shown in Figure 5B in the following order: HAP-40 nm > HAP-70 nm > HAP-1 μm > HAP-2 μm > control group.

3.5. HAP Induces Apoptosis and Necrosis of HK-2 Cells. Hoechst 33342 can penetrate the cell membrane, enter normal and apoptotic cells, combine with DNA, and display blue fluorescence under ultraviolet light, and the fluorescence of apoptotic cells after staining is significantly enhanced compared with that of normal cells.[21,22] Propidium iodide (PI) cannot penetrate cell membranes and cannot stain normal cells or apoptotic cells with an intact cell membrane. However, the integrity of the cell membrane of necrotic cells is lost, and PI can penetrate the cell membrane to stain the necrotic cells and produce red fluorescence. Figure 6 presents the apoptotic and necrotic cells detected after Hoechst 33342 and PI double staining.

The number of stained cells (blue and red) in the control group was less than that in the HAP crystal group, and the red- and blue-stained cells in the HAP crystal group were greater than those in the control group. However, the number of blue-stained cells in the nano-HAP group was much greater than that of the red-stained cells. The results indicated that nano-/micro-HAP crystals caused apoptosis and necrosis, and the degree of cell death caused by nano-HAP crystals was greater than that induced by micro-HAP crystals. In Figure 6, the intensity of blue fluorescence was relatively uniform, whereas the size of red fluorescence varied greatly because of the swelling of necrotic cells.

3.6. Observation of the Adhesion of HAP Crystals on the Cell Surface. An optical microscope was used to observe the adhesion of HAP crystals to HK-2 cells (Figure 7). A large number of HAP crystals adhered to the cell surface. When the size of the crystals was much small (such as HAP-40 nm), the crystals appeared as small black spots because nanocrystals have a strong absorbance.[23] Nanocrystals also cause aggregation on the cell surface because of their high surface energy.

In the presence of a fixed crystal concentration (250 μg/mL), a few cells had shiny crystals on their surfaces because of the small number of micro-HAP crystals. By contrast, nano-HAP crystals adhered to almost every cell.

3.7. Quantitative Detection of HAP Adhesion Amount on Cell Surface. The amount of HAP crystals that adhered to the cell surface was quantitatively detected by flow cytometry (Figure 8A). The proportion of cells adhering to crystals is HAP-40 nm (97.0%) > HAP-70 nm (91.1%) > HAP-1 μm (83.7%) > HAP-2 μm (74.4%), that is, the smaller the size of HAP crystals, the greater the proportion of cells adhering to crystals (Figure 8B). The curve of correlation between the adhesion amount of crystals and HA expression is presented in Figure 8C (R^2 = 0.9448). The proportion of cells adhering to crystals was positively correlated with the expression of HA on the cell surface.

3.8. Quantitative Detection of the Amount of HK-2 Cells That Endocytosed Different Sizes of HAP. After the crystals that adhered to the cell surface were removed with EDTA,[16] the proportion of cells endocytosing the crystals was detected through flow cytometry (Figure 9A). The cells with an FITC signal could be regarded as cells with endocytic crystals. All four sizes of HAP crystals could be endocytosed by HK-2 cells, and the proportion of cells with endocytic crystals changed in a size-dependent manner. The proportion of cells endocytosing HAP crystals was as follows: HAP-40 nm (46.6%) > HAP-70 nm (28.8%) > HAP-1 μm (12.4%) > HAP-2 μm (7.08%) > control group (0.38%; Figure 9B). This result indicated that the smaller the crystal size, the easier endocytosis.

https://doi.org/10.1021/acsomega.3c08180
ACS Omega 2023, 8, 48432−48443

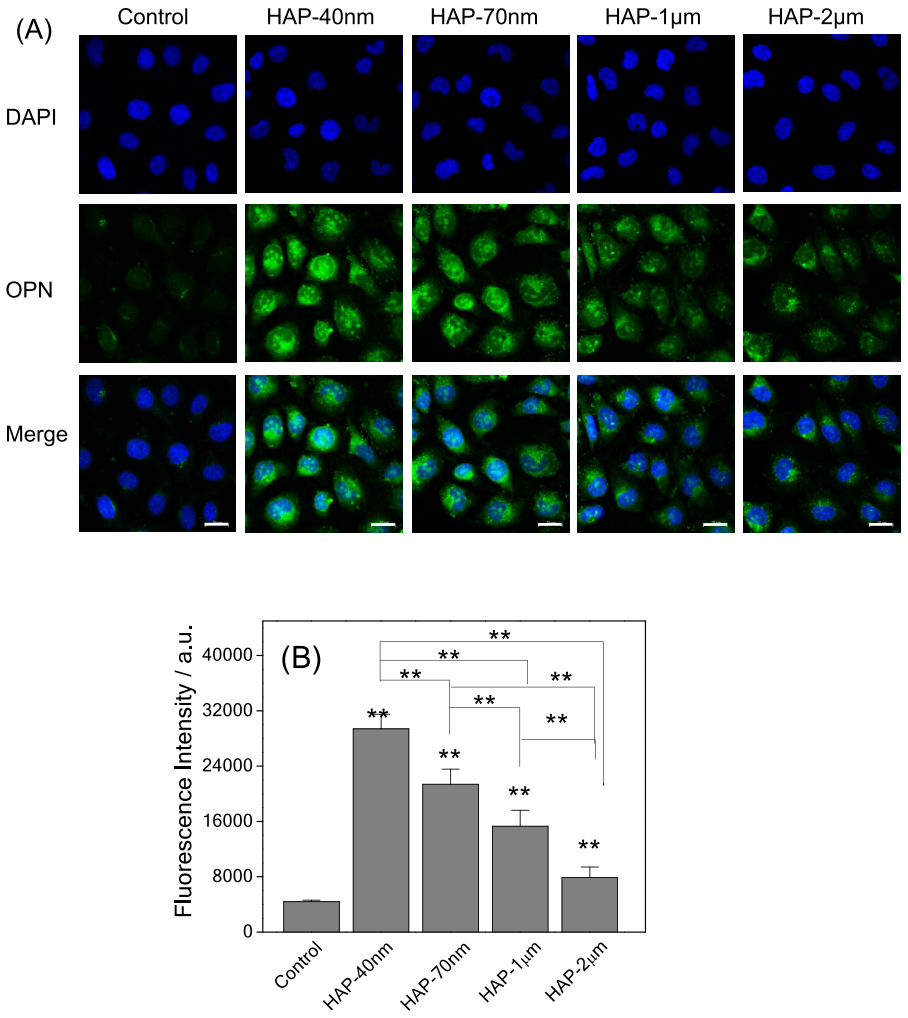

Figure 3. OPN expression of HK-2 cells after the treatment with HAP with different sizes. (A) Fluorescence observation of the OPN expression. (B) Quantitative histogram of the OPN expression. Crystal concentration: 250 μg/mL; treatment time: 24 h. Green fluorescence: OPN; blue fluorescence: cell nucleus. Scale bars: 20 μm.

3.9. Distribution of HAP Crystals Inside and Outside the Cell Membrane. As shown in Figure 10, the smallest HAP crystal, i.e., HAP-40 nm, was mostly endocytosed by the cells, and only a small part adhered to the outer part of the cell membrane. However, the largest HAP crystal, i.e., HAP-2 μm, mainly adhered to the outer part of the cell, and a few crystals entered the cell membrane. This result suggested that the degree of endocytosis of nanocrystals by HK-2 cells was obviously greater than that of microcrystals, but the adhesion of microcrystals was greater than that of nanocrystals.

The difference in crystal size (green fluorescence) observed in Figure 10 was not large because the nano-HAP crystals had a low absolute zeta potential (3.21−4.14 mV) in the culture solution (Table 1). After entering the cells, nano-HAP crystals would aggregate, so the observed size was much larger than the actual size of a single nanocrystal.[24,25] By contrast, the absolute Zeta potential (13.94−24.08 mV) of micro-HAP crystals was higher than that of nano-HAP crystals, and the dispersion of the former was better than that of the latter.

3.10. Detection of Wound Healing Abilities after HK-2 Cells Endocytosed Different Sizes of HAP. Cell migration is a mechanical integration process involving dynamic changes in cell adhesion, cytoskeletal organization, and signal transduction. Cell migration is involved in various physiological and pathological processes. The endocytosis of crystals affects a series of biological behaviors, including cell growth, apoptosis, and migration.[26,27]

Figure 11 shows wound healing abilities before and after HK-2 cells endocytose different sizes of HAP crystals observed under the microscope. After 48 h, the scratch spacing of the cells in the control group decreased obviously, indicating that the cell migration rate of the control group was the fastest. By contrast, the healing of the scratches in the crystal treatment groups was slower than that in the control group. The healing speed of scratches within 48 h showed the following order (Table 2): HAP-40 nm (10.6 μm·h^{-1}) < HAP-70 nm (11.8 μm·h^{-1}) < HAP-1 μm (15.2 μm·h^{-1}) < HAP-2 μm (15.3 μm·h^{-1}) < control (33.7 μm·h^{-1}).

4. DISCUSSION

4.1. Influencing Factors of HAP Crystal Adhesion and Endocytosis in HK-2 Cells. Crystal size and surface properties play a key role in their interaction with cells.[28] The adhesion of HAP to cells is fast and can reach a stable state within a few minutes.[29] However, the endocytosis of crystals consists of two processes. First, crystals interact with lipids and proteins on the cell membrane by adhering to cells. Then, these crystals are internalized and further transported to different subcellular

https://doi.org/10.1021/acsomega.3c08180
ACS Omega 2023, 8, 48432−48443

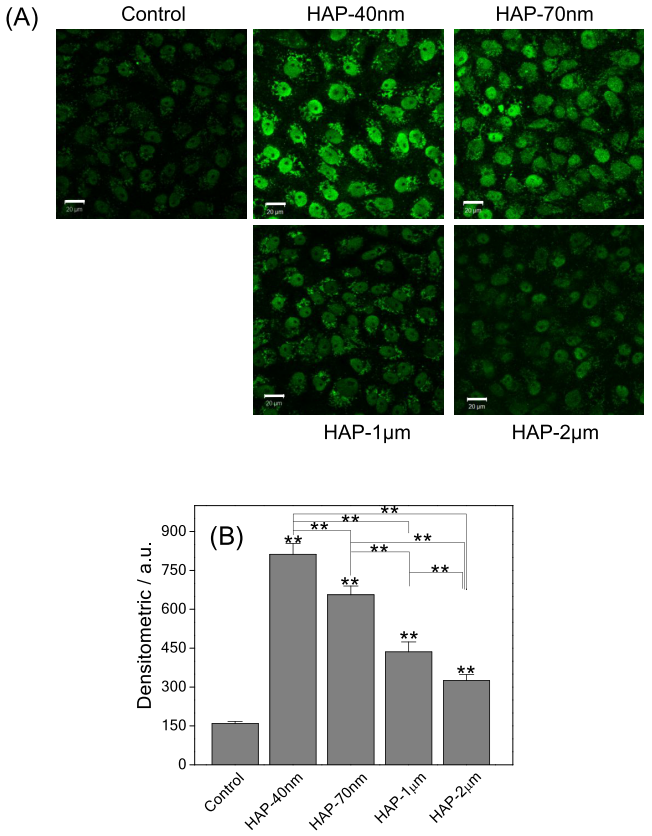

Figure 4. Hyaluronic acid expression of HK-2 cells after the treatment of HAP with different sizes. (A) Laser confocal microscopy image. (B) Quantitative analysis of relative fluorescence intensity. Crystal concentration: 250 μg/mL; treatment time: 24 h. Scale: 20 μm. Compared with the control group, $^{*}P < 0.05$, $^{**}P < 0.01$.

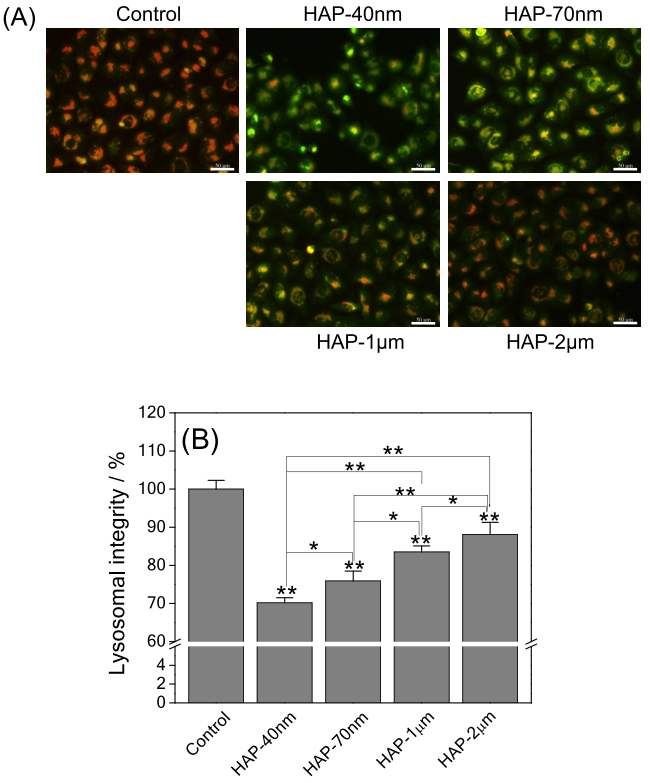

Figure 5. Changes in lysosomal integrity of HK-2 cells after the treatment of HAP with different sizes. (A) Fluorescence microscopy images. (B) Quantitative histogram of lysosomal integrity. Red fluorescence: lysosome. Crystal concentration: 250 μg/mL; treatment time: 24 h. Scale bars: 20 μm. Compared with the control group, $^{*}P < 0.05$, $^{**}P < 0.01$.

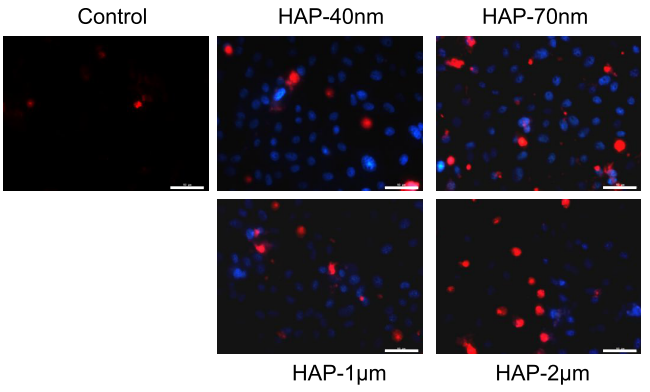

Figure 6. Apoptosis and necrosis observation using Hoechst 33342 and PI double staining of HK-2 cells after the treatment with HAP with different sizes. Crystal concentration: 250 μg/mL; treatment time: 24 h.

organelles under the control of energy.[30,31] The adhesion of cells to HAP is an important step in endocytosis efficiency. Figure 12 shows a mechanical schematic of the adhesion and endocytosis of HAP crystals with different sizes in HK-2 cells.

4.1.1. Specific Surface Area. Small crystals have a large specific surface area (S_{BET}), and the S_{BET} of the crystals showed the following order: HAP-40 nm (76.2 m^2/g) > HAP-70 nm (67.0 m^2/g) > HAP-1 μm (6.16 m^2/g) > HAP-2 μm (1.18 m^2/g, Table 1). Therefore, nano-HAP crystals were more likely to come in contact with cells than micro-HAP crystals, and the proportion of nano-HAP crystals adhering to cells was greater than that of micro-HAP crystals. The high adhesion of the cells to the HAP crystals improved the endocytosis efficiency of the cells with respect to the HAP crystals.

4.1.2. Number of Crystal Particles. Under the same mass concentration (250 μg/mL), the number of nano-HAP crystals was much larger than that of micro-HAP crystals. Therefore, the probability of nano-HAP adhering to the cells and endocytosing by the cells is significantly increased compared with micro-HAP (Figures 8 and 9).

4.1.3. Zeta Potential. The membrane surface of most cells has a large area of negatively charged regions,[32] so repulsion between cells and crystals with a more negative Zeta potential increases. In the medium used in this study, the Zeta potentials of the HAP crystals were as follows (Table 1): HAP-40 nm (−3.21 mV) > HAP-70 nm (−4.14 mV) > HAP-1 μm (−13.94 mV) > HAP-2 μm (−24.08 mV). This result indicated that the repulsion between nano-HAP and cells is much smaller than that between micro-HAP crystals and cells, which makes the adhesion ability between nano-HAP and cells significantly enhanced.

4.1.4. Contact Angle and Contact Interface. In Figure 2, as the size of the HAP crystals increased, the contact angle of the crystals increased, resulting in weakening of the adhesion ability between the crystals and the cells. This phenomenon occurred because the adhesion properties of a material are closely related to shear stress.[33] As crystal size increases, the degree of the contact interface between crystals and cells decreases, and the critical shear force decreases; as a result, the adhesion force of cells to large crystals weakens.[34]

https://doi.org/10.1021/acsomega.3c08180
ACS Omega 2023, 8, 48432−48443

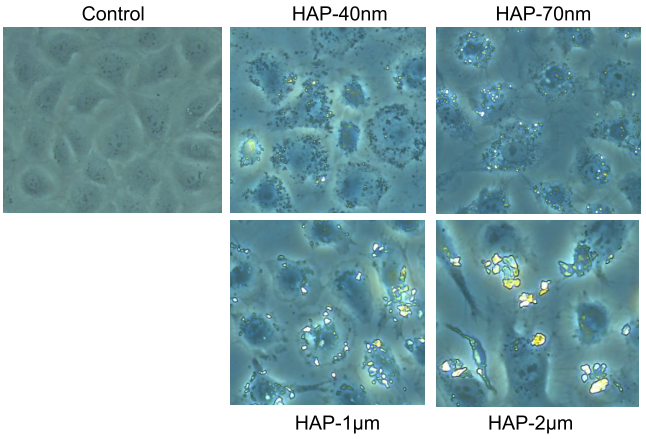

Figure 7. Microscope observation of the adhesion of HAP crystals with different sizes on the cell surface. Crystal concentration: 250 μg/mL; treatment time: 24 h.

4.1.5. Expression of Adhesion Molecules. Important adhesion molecules on the cell surface (OPN, HA) can combine with calcium ions, calcium oxalate crystals, and HAP crystals in urine.[35] The upregulation of the expression levels of the molecules of OPN, HA, and other molecules can promote the adhesion and endocytosis of crystals, thereby accelerating kidney stone formation. In this study, the ability of nano-HAP crystals to promote the OPN (Figure 3) and HA (Figure 4) expression levels in the cells were greater than those of micro-HAP crystals. Therefore, the adhesion and endocytosis amounts of HAP crystals decreased as the crystal size increased (Figures 8 and 9). In addition, the adhesion amount was positively correlated with the expression level of adhesion molecules, such as HA, on the cell surface (correlation coefficient R^2 = 0.9448, Figure 8B). Zhang et al.[36] showed that the amount of 80 nm-diameter spherical SiO_2 particles that adhere to human skin fibroblasts is greater than 500 nm because of the high impedance of large SiO_2 particles to cell adhesion.

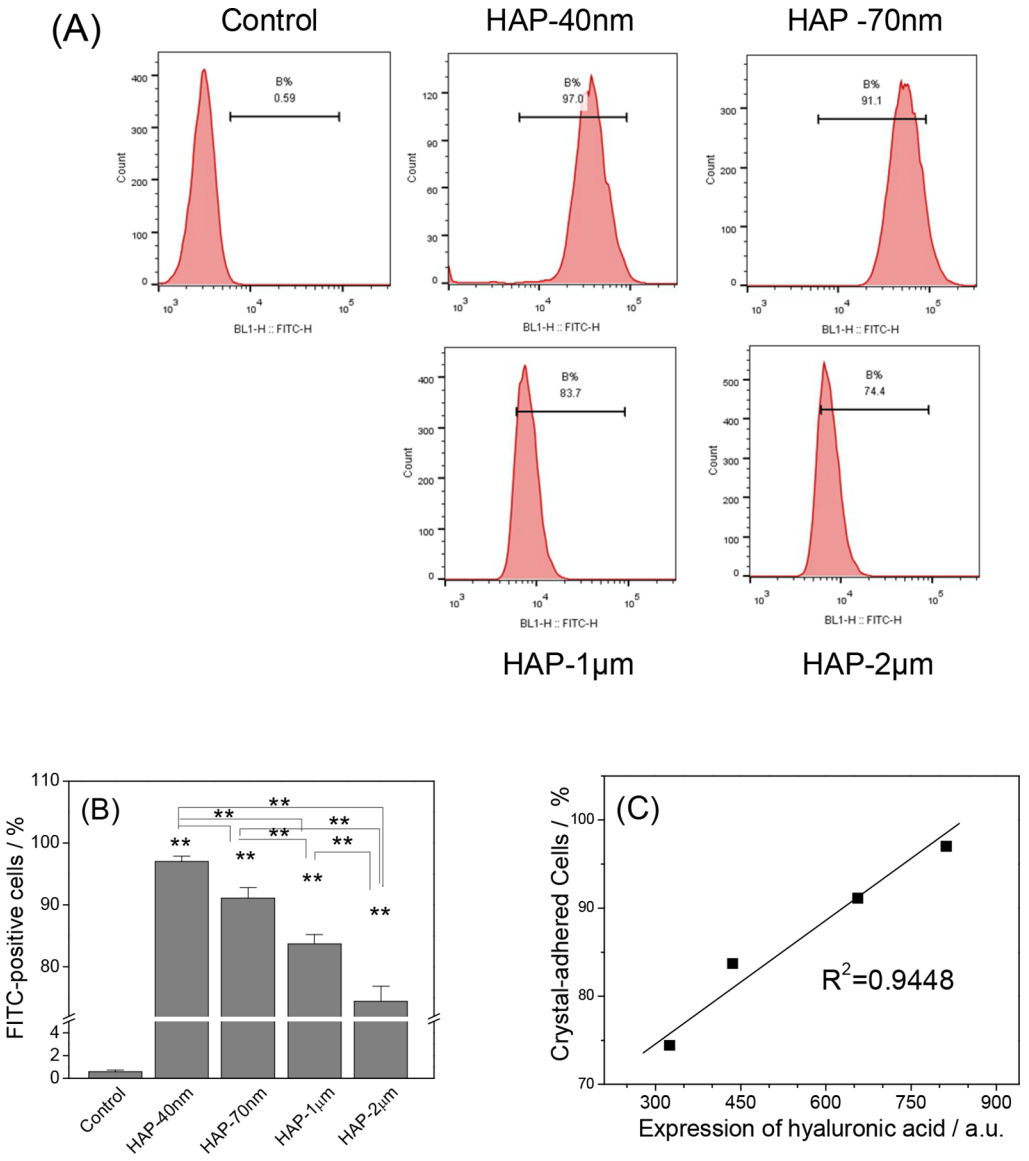

Figure 8. Quantitative detection of the proportion of cells with adhered HAP crystals by flow cytometry. (A) Histogram of the proportion of cells with adhered HAP crystals. (B) Quantitative histogram. (C) The correlation curve is between the adhesion ratio of crystals and HA expression. R^2 is the linear correlation coefficient. Crystal concentration: 250 μg/mL; treatment time: 24 h. Compared with the control group, $^*P < 0.05$; $^{**}P < 0.01$.

https://doi.org/10.1021/acsomega.3c08180
ACS Omega 2023, 8, 48432−48443

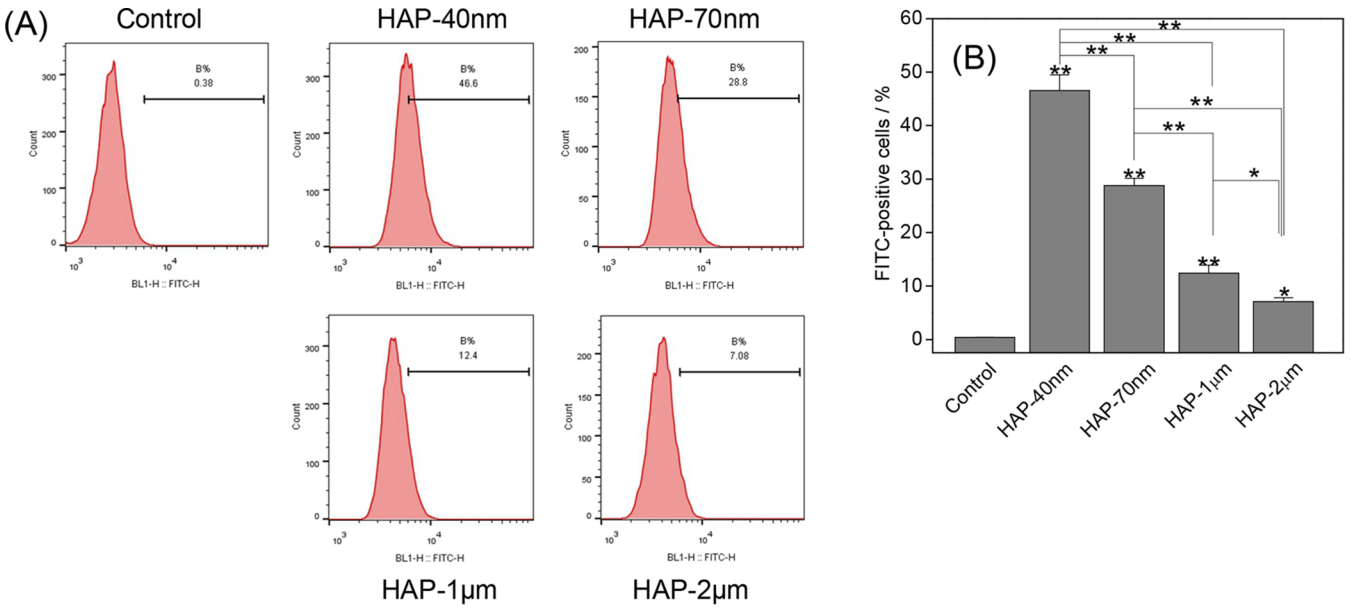

Figure 9. Quantitative detection of the proportion of cells with endocytosed HAP crystals by flow cytometry. (A) Histogram of the proportion of cells with endocytosed HAP crystals. (B) Statistical results of the proportion of cells with endocytosed HAP crystals. Crystal concentration: 250 μg/mL; treatment time: 24 h. Compared with the control group, $^{*}P < 0.05$; $^{**}P < 0.01$.

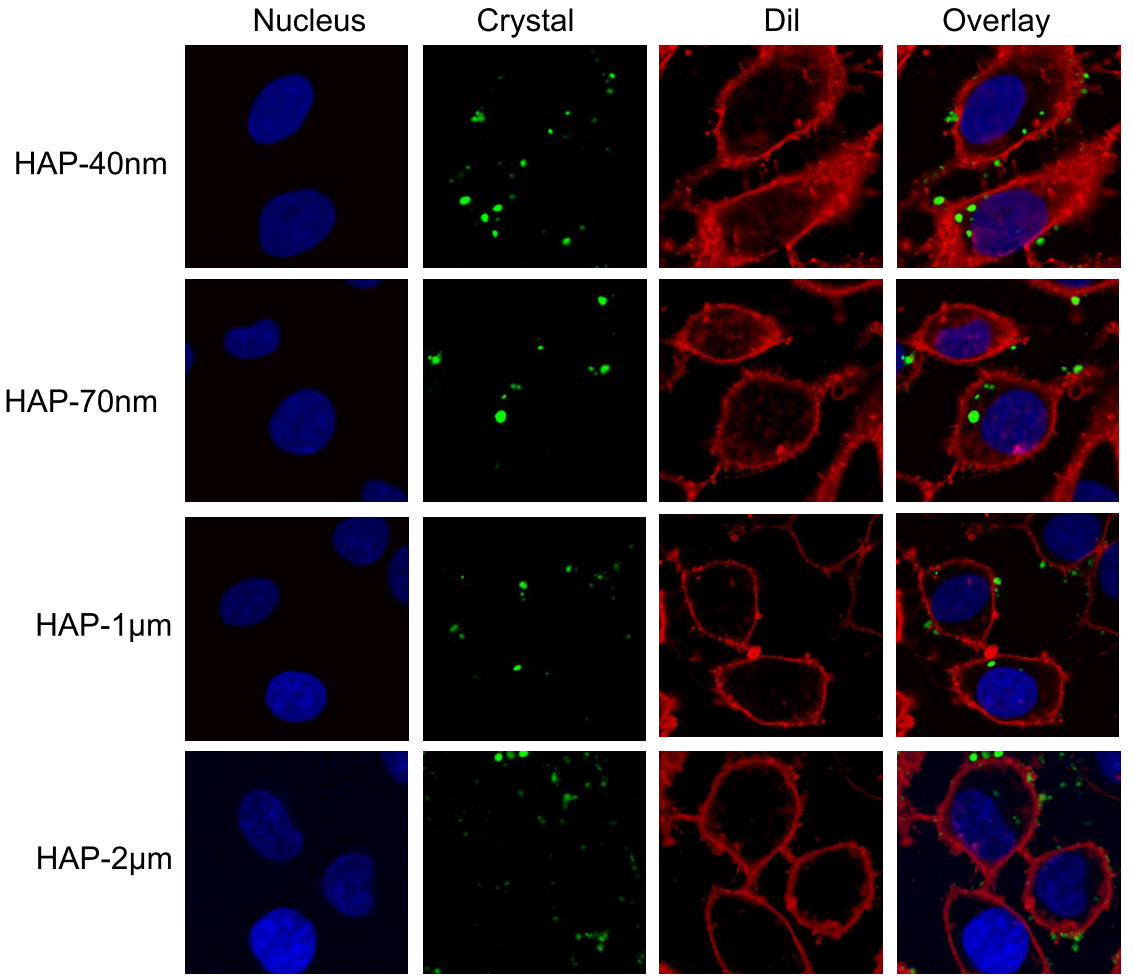

Figure 10. Laser scanning confocal images of the distribution of different sizes of HAP crystals inside and outside of the HK-2 cells. HAP crystals (green) were labeled by FITC, and the cell nucleus (blue) and cell membrane (red) were labeled by DAPI and DiI. Crystal concentration: 250 μg/mL, treatment time: 24 h.

https://doi.org/10.1021/acsomega.3c08180
ACS Omega 2023, 8, 48432−48443

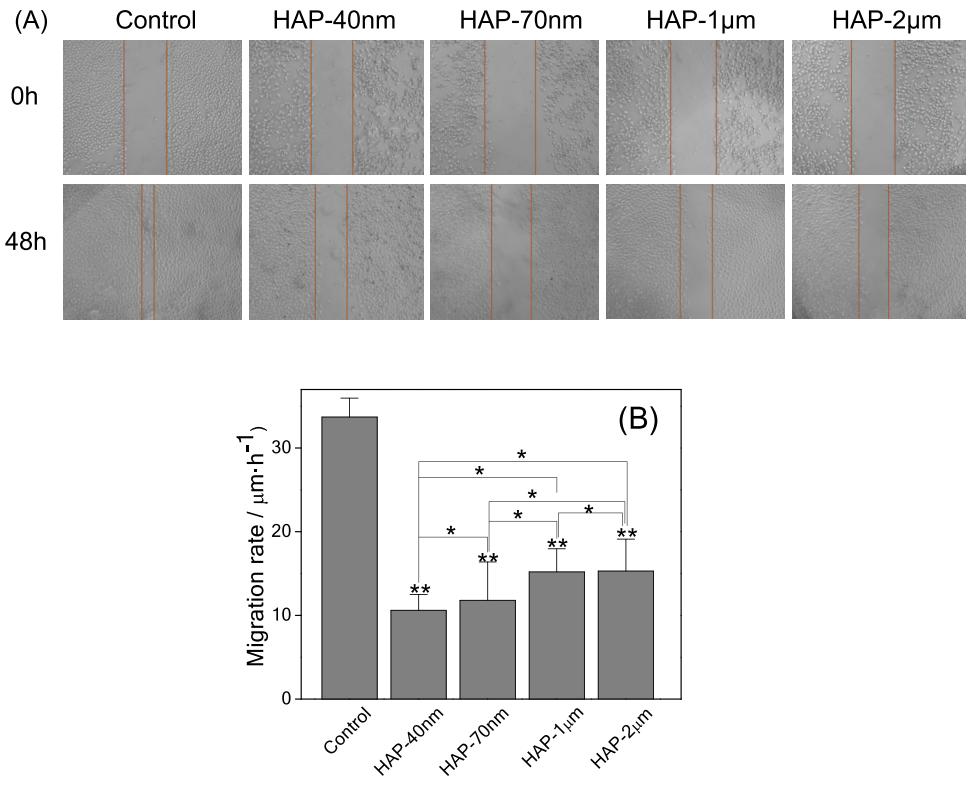

Figure 11. Effects of different sizes of HAP crystals on cell migration of HK-2 cells. (A) Microscope images (×100). (B) Statistical results of cell migration speed within 48 h. Crystal concentration: 250 μg/mL.

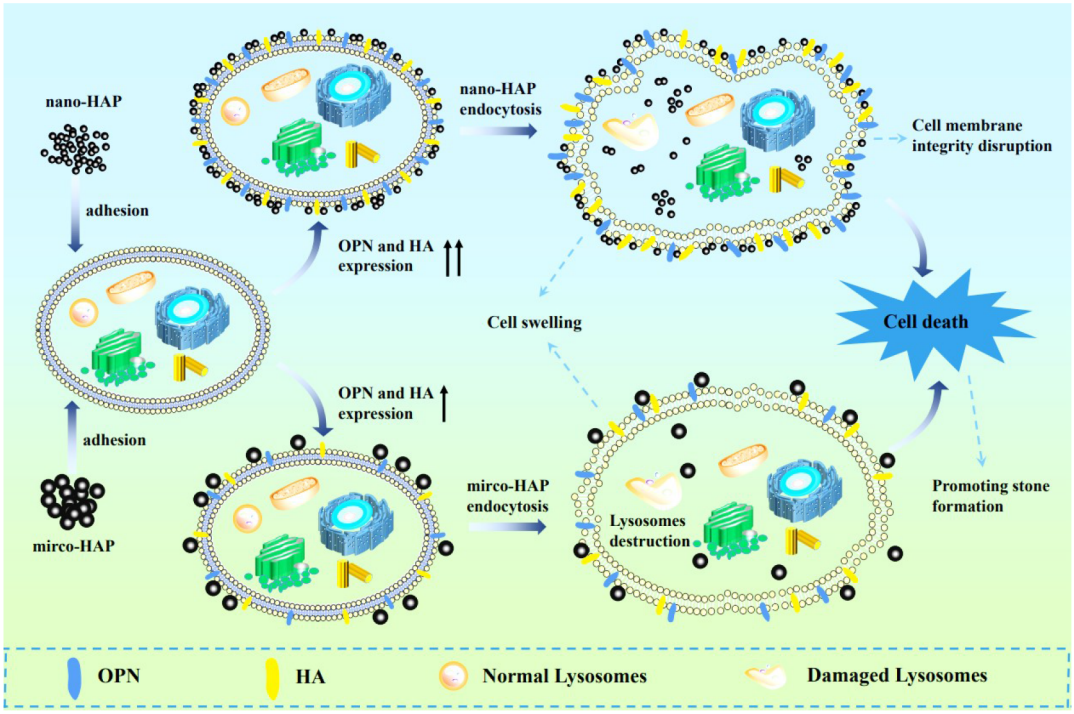

Figure 12. Model diagram of the adhesion and endocytosis of different sizes of HAP crystals in HK-2 cells.

4.2. Effect of Adhesion and Endocytosis on the Cytotoxicity of HAP Crystals. *4.2.1. Cell Migration Rate.* Cell adhesion is essential for controlling multiple cell functions, including cell growth, migration, and differentiation. After cells interact with crystals, the migration rate of cells is affected by crystal size.[37] Scratch healing is a common result of cell proliferation and migration. In this study, the cells in the nano-HAP treatment group were severely damaged, and their migration rate was slower than that in the micro-HAP treatment group. However, the cells in the micro-HAP treatment group were relatively less damaged than those in the nano-HAP treatment groups, so the self-repair and migration rates of the

https://doi.org/10.1021/acsomega.3c08180
ACS Omega 2023, 8, 48432−48443

Table 2. Migration Speed of HK-2 Cells after the Treatment of HAP with Different Sizes

crystal	scratch distance/mm (0 h)	scratch distance/mm (48 h)	migration distance/mm (48 h)	migration speed/μm/h (48 h)
control	226.06	64.33	161.73	33.7
HAP-40 nm	220.86	169.98	50.88	10.6
HAP-70 nm	268.35	211.51	56.84	11.8
HAP-1 μm	241.27	168.28	72.99	15.2
HAP-2 μm	231.18	157.82	73.36	15.3

cells were also faster (Figure 11). This result indicated that the migration rate was negatively related to cytotoxicity. The highly toxic TiO_2 particles are more capable of inhibiting cell migration.[38] However, some studies[39] have shown that mesoporous SiO_2 spherical nanoparticles can increase the cell migration rate. Inconsistent results may be related to cell lines, particles, and evaluation methods used in a given study.

4.2.2. Cytotoxicity. During cell adhesion and uptake, morphological changes and cytoskeletal disintegration may occur, causing damage to cell membranes (Figure 7) and subcellular organelles. Nano-HAP crystals damaged cells to a greater extent than micro-HAP crystals did (Figure 5). Nano-HAP crystals also slowed the rate of cell wound healing (Figure 11) and induced apoptosis and necrosis (Figure 6). Yuan et al.[40] showed that the effect of nano-HAP particles on HepG2 cell viability depends obviously on particle size, and the effect on cell apoptosis increases as particle size decreases.

Endocytosed crystals are the key cause of cytotoxicity. The number of internalized exogenous particles is highly correlated with cytotoxicity. The endocytosis of crystals by cells may be an important reason for nano-HAP toxicity.[26,30] In the present study, the proportion of cells endocytosing crystals also decreased as the size of the endocytosed crystals increased. Yin et al.[41] showed that the effective uptake of HAP in Bel-7402 cells through endocytosis may seriously affect cell membrane integrin, influence cell proliferation, and cause cell death. The correlation between cytotoxicity and endocytosis was higher than that of the amount of adhesion crystals in cells, indicating that endocytosed crystals were the key cause of cytotoxicity. Endocytosed crystals can directly act on subcellular organelles,[35] causing more direct apoptosis and necrosis. Furthermore, endocytosis is closely related to the crystal size. The uptake of small gold nanoparticles is high in Hela cells.[42] Shi et al.[29] studied the adhesion and endocytosis of different sizes (20 nm, 80 nm, and 12 μm) of HAP by human umbilical cord Wharton's jelly-derived mesenchymal stem cells (hWJ-MSCs). They found that nanoscale HAP crystals easily adhere to the cell membrane and become endocytosed, but micro-HAP crystals with a low surface energy have a low degree of adhesion.

Relatively more nano-HAP crystals were endocytosed (Figure 9) and accumulated in the cells (Figure 10). However, micro-HAP crystals were mostly outside the cell membrane and adhered to the cell membrane (Figure 10). Micro-HAP crystals mainly adhered to the surface of the HK-2 cells and induced damage to the cell organelles by disrupting the cell membrane. However, nano-HAP crystals could damage the cell membrane and enter the cells to directly destroy organelles, causing greater cell damage, apoptosis, and necrosis (Figure 12).[43] After HK-2 cells were injured by HAP, the adhesion and aggregation abilities of the crystals to the cells increased. Consequently, Randall plaque formation was promoted, and CaOx stone formation was induced.

5. CONCLUSIONS

The adhesion and endocytosis of HAP crystals in HK-2 cells are closely related to the crystal size. The ability of the cells to adhere to and endocytose crystals increased as the crystal size decreased. Micro-HAP crystals mainly produce cytotoxicity by damaging the cell membrane. Conversely, nano-HAP crystals could adhere to the cell surface, damage the cell membrane, and be endocytosed by the cells. As a result, the subcellular organelles were directly damaged. Therefore, nano-HAP crystals were more toxic to HK-2 cells than micro-HAP crystals. The adhered HAP crystals promoted the expression of OPN and HA on the cell surface. Consequently, the abilities of the cells to adhere to and endocytose crystals were enhanced, and the apoptosis and necrosis rates of the cells increased. This study could help further understand the role of HAP crystals in the Randall plaque formation and CaOx stone formation.

AUTHOR INFORMATION

Corresponding Authors

Jian-Ming Ouyang − *Department of Chemistry, Institute of Biomineralization and Lithiasis Research, Jinan University, Guangzhou, Guangdong 510632, China*; orcid.org/0000-0001-8075-3915; Email: toyjm@jnu.edu.cn

Bao-Song Gui − *Department of Nephrology, The Second Affiliated Hospital, Xi'an Jiaotong University, Xi'an 710004, China*; Email: guibsdoctor@sina.com

Authors

Jin Han − *Department of Nephrology, The Second Affiliated Hospital, Xi'an Jiaotong University, Xi'an 710004, China*

Xin-Yi Tong − *Department of Chemistry, Institute of Biomineralization and Lithiasis Research, Jinan University, Guangzhou, Guangdong 510632, China*

Chen-Ying Rao − *Department of Chemistry, Institute of Biomineralization and Lithiasis Research, Jinan University, Guangzhou, Guangdong 510632, China*

Complete contact information is available at: https://pubs.acs.org/10.1021/acsomega.3c08180

Notes

The authors declare no competing financial interest.

ACKNOWLEDGMENTS

This work was supported by the National Key R&D Plan (No. 2020YFC2002700), the National Natural Science Foundation of China (No. 82270800), and Zhongguancun Nephrology & Blood Purification Innovation Alliance, Youth Fund Project of CKD-MBD(NBPIA20QC0201).

REFERENCES

(1) Canela, V. H.; Bledsoe, S. B.; Worcester, E. M.; Lingeman, J. E.; El-Achkar, T. M.; Williams, J. C. Collagen fibrils and cell nuclei are entrapped within Randall's plaques but not in CaOx matrix overgrowth: A microscopic inquiry into Randall's plaque stone pathogenesis. *Anat. Rec.* **2022**, *305* (7), 1701−1711.

(2) Makki, M. S.; Winfree, S.; Lingeman, J. E.; Witzmann, F. A.; Worcester, E. M.; Krambeck, A. E.; Coe, F. L.; Evan, A. P.; Bledsoe, S.; Bergsland, K. J.; Khochare, S.; Barwinska, D.; Williams, J. C.; El-Achkar, T. M. A precision medicine approach uncovers a unique signature of

https://doi.org/10.1021/acsomega.3c08180
ACS Omega 2023, 8, 48432−48443

neutrophils in patients with brushite kidney stones. *Kidney Int. Rep.* **2020**, *5* (5), 663−677.
(3) Lee, T.; Lin, Y. C. Mimicking the initial development of calcium urolithiasis by screening calcium oxalate and calcium phosphate phases in various urinelike solutions, time points, and pH values at 37°C. *Cryst. Growth Des.* **2011**, *11* (7), 2973−2992.
(4) Alelign, T.; Petros, B. Kidney stone disease: an update on current concepts. *Adv. Urol.* **2018**, *2018*, No. 3068365.
(5) Liu, H.; Huang, L.-H.; Sun, X.-Y.; Ouyang, J.-M. High-phosphorus environment promotes calcification of A7R5 cells induced by hydroxyapatite nanoparticles. *Mater. Sci. Eng., C* **2020**, *107*, No. 110228.
(6) Gao, J.; Xue, J.-F.; Xu, M.; Gui, B.-S.; Wang, F.-X.; Ouyang, J.-M. Nanouric acid or nanocalcium phosphate as central nidus to induce calcium oxalate stone formation: a high resolution transmission electron microscopy study on urinary nanocrystallites. *Int. J. Nanomed.* **2014**, *9*, 4399−4409.
(7) Grases, F.; Costa-Bauzá, A.; Gomila, I.; Ramis, M.; García-Raja, A.; Prieto, R. M. Urinary pH and renal lithiasis. *Urol. Res.* **2012**, *40*, 41−46.
(8) Ahmatjan, B.; Ruotian, L.; Rahman, A.; Bin, M.; Heng, D.; Yi, H.; Tao, C.; Le, G.; Mahmut, M. Klotho inhibits the formation of calcium oxalate stones by regulating the Keap1-Nrf2-ARE signaling pathway. *Int. Urol. Nephrol.* **2023**, *55*, 263.
(9) Wang, B. H.; Wei, J. C.; Qi, H. F.; Fei, G.; Qin, L. X.; Jiao, Z.; Wen, J. M.; Ye, Z. Q.; Yang, X. Q.; Liu, H. R. Identification of Resolvin D1 and Protectin D1 as Potential Therapeutic Agents for Treating Kidney Stones. *Oxid. Med. Cell. Longevity* **2022**, *2022*, No. 4345037.
(10) Cheunsuchon, B.; Sritippayawan, S. Successful treatment of early allograft dysfunction with cinacalcet in a patient with nephrocalcinosis caused by severe hyperparathyroidism: a case report. *BMC Res. Notes* **2017**, *10* (1), 153.
(11) Liu, J. N.; Yang, K.; Jin, Y. S.; Liu, Y. D.; Chen, Y. D.; Zhang, X. H.; Yu, S. L.; Song, E. L.; Chen, S.; Zhang, J. B.; Jing, G. H.; An, R. H. H3 relaxin protects against calcium oxalate crystal-induced renal inflammatory pyroptosis. *Cell Proliferation* **2020**, *53* (10), No. e12902.
(12) Hovda, K. E.; Guo, C.; Austin, R.; Ke, M. M. Renal toxicity of ethylene glycol results from internalization of calcium oxalate crystals by proximal tubule cells. *Toxicol. Lett.* **2010**, *192* (3), 365−372.
(13) Shi, X.; Zhou, K.; Huang, F.; Wang, C. Interaction of hydroxyapatite nanoparticles with endothelial cells: internalization and inhibition of angiogenesis in vitro through the PI3K/Akt pathway. *Int. J. Nanomed.* **2017**, *12*, 5781−5795.
(14) Dominska, M.; Dykxhoorn, D. M. Breaking down the barriers: siRNA delivery and endosome escape. *J. Cell Sci.* **2010**, *123* (8), 1183−1189.
(15) Huang, L.-H.; Han, J.; Ouyang, J.-M.; Gui, B.-S. Shape-dependent adhesion and endocytosis of hydroxyapatite nanoparticles on A7R5 aortic smooth muscle cells. *J. Cell. Physiol.* **2020**, *235*, 465−479.
(16) Lesniak, A.; Salvati, A.; Santos-Martinez, M. J.; Radomski, M. W.; Dawson, K. A.; Aberg, C. Nanoparticle adhesion to the cell membrane and its effect on nanoparticle uptake efficiency. *J. Am. Chem. Soc.* **2013**, *135* (4), 1438−1444.
(17) Surmeneva, M. A.; Kleinhans, C.; Vacun, G.; Kluger, P. J.; Schönhaar, V.; Müller, M.; Hein, S. B.; Wittmar, A.; Ulbricht, M.; Prymak, O.; Oehr, C.; Surmenev, R. A. Nano-hydroxyapatite-coated metal-ceramic composite of iron-tricalcium phosphate: Improving the surface wettability, adhesion and proliferation of mesenchymal stem cells in vitro. *Coll. Surf. B* **2015**, *135*, 386−393.
(18) Qi, S.; Wang, Q.; Xie, B.; Chen, Y.; Zhang, Z.; Xu, Y. P38 MAPK signaling pathway mediates COM crystal-induced crystal adhesion change in rat renal tubular epithelial cells. *Urolithiasis* **2020**, *48* (1), 9−18.
(19) Chen, S.; Zhou, C.; Yu, H.; Tao, L.; An, Y.; Zhang, X.; Wang, Y.; Wang, Y.; Xiao, R. 27-Hydroxycholesterol contributes to lysosomal membrane permeabilization-mediated pyroptosis in co-cultured SH-SY5Y cells and C6 cells. *Front. Mol. Neurosci.* **2019**, *12*, 14.
(20) Qiu, K.; Zhu, H.; Rees, T. W.; Ji, L.; Zhang, Q.; Chao, H. Recent advances in lysosome-targeting luminescent transition metal complexes. *Coordin. Chem. Rev.* **2019**, *398*, 113010.
(21) Li, W.; Yue, X.; Li, F. Gallic acid caused cultured mice TM4 Sertoli cells apoptosis and necrosis. *Asian. Austral. J. Anim.* **2019**, *32* (5), 629−636.
(22) Fang, J.; Zhao, X.; Li, S.; Xing, X.; Wang, H.; Lazarovici, P.; Zheng, W. Protective mechanism of artemisinin on rat bone marrow-derived mesenchymal stem cells against apoptosis induced by hydrogen peroxide via activation of c-Raf-Erk1/2-p90(rsk)-CREB pathway. *Stem Cell Res. Ther.* **2019**, *10* (1), 312.
(23) Kundu, S.; Patra, A. Nanoscale Strategies for Light Harvesting. *Chem. Rev.* **2017**, *117* (2), 712−757.
(24) Ashraf, M. A.; Peng, W.; Zare, Y.; Rhee, K. Y. Effects of size and aggregation/agglomeration of nanoparticles on the interfacial/interphase properties and tensile strength of polymer nanocomposites. *Nanoscale Res. Lett.* **2018**, *13* (1), 214.
(25) Wu, M.; Guo, H.; Liu, L.; Liu, Y.; Xie, L. Size-dependent cellular uptake and localization profiles of silver nanoparticles. *Int. J. Nanomedicine* **2019**, *14*, 4247−4259.
(26) Seike, S.; Miyamoto, K.; Kobayashi, K.; Takehara, M.; Nagahama, M. Clostridium perfringens delta-toxin induces rapid cell necrosis. *PLoS One* **2016**, *11* (1), No. e0147957.
(27) Rauwel, E.; Al-Arag, S.; Salehi, H.; Amorim, C. O.; Cuisinier, F.; Guha, M.; Rosario, M. S.; Rauwel, P. Assessing cobalt metal nanoparticles uptake by cancer cells using live raman spectroscopy. *Int. J. Nanomed.* **2020**, *15*, 7051−7062.
(28) Liao, F.; Chen, L.; Liu, Y.; Zhao, D.; Peng, W.; Wang, W.; Feng, S. The size-dependent genotoxic potentials of titanium dioxide nanoparticles to endothelial cells. *Environ. Toxicol.* **2019**, *34* (11), 1199−1207.
(29) Shi, X.; Zhou, K.; Huang, F.; Zhang, J.; Wang, C. Endocytic mechanisms and osteoinductive profile of hydroxyapatite nanoparticles in human umbilical cord Wharton's jelly-derived mesenchymal stem cells. *Int. J. Nanomed.* **2018**, *13*, 1457−1470.
(30) Thongboonkerd, V. Proteomics of crystal-cell interactions: A model for kidney stone research. *Cells* **2019**, *8* (9), 1076.
(31) Helaine, C.; Ozcelik, H.; Komaty, S.; Amedlous, A.; Ghojavand, S.; Goux, D.; Retoux, R.; Mintova, S.; Valable, S. Internalization study of nanosized zeolite crystals in human glioblastoma cells. *Colloids Surf., B* **2022**, *218*, No. 112732.
(32) Banerjee, T.; Biswas, D.; Pal, D. S.; Miao, Y. C.; Iglesias, P. A.; Devreotes, P. N. Spatiotemporal dynamics of membrane surface charge regulates cell polarity and migration *Nat. Cell Biol.* **2022**, *24*(10), 1499, DOI: 10.1038/s41556-022-00997-7.
(33) Araujo, D.; Alves, V. D.; Campos, J.; Coelhoso, I.; Sevrin, C.; Grandfils, C.; Freitas, F.; Reis, M. A. Assessment of the adhesive properties of the bacterial polysaccharide FucoPol. *Int. J. Biol. Macromol.* **2016**, *92*, 383−389.
(34) Patil, V. R. S.; Campbell, C. J.; Yun, Y. H.; Slack, S. M.; Goetz, D. J. Particle diameter influences adhesion under flow. *Biophys. J.* **2001**, *80* (4), 1733−1743.
(35) Cao, L. H.; Chen, Q.; Chen, J.; Chen, W. M. Irbesartan inhibits the formation of calcium oxalate stones in the kidney of diabetic rats. *Int. J. Clin. Exp. Med.* **2018**, *11* (3), 1726−1733.
(36) Zhang, Y.; Hu, L.; Yu, D. H.; Gao, C. Y. Influence of silica particle internalization on adhesion and migration of human dermal fibroblasts. *Biomaterials* **2010**, *31* (32), 8465−8474.
(37) Mkandawire, M. M. Induction of apoptosis in human cancer cells by targeting mitochondria with gold nanoparticles. *Nanoscale* **2015**, *7* (24), 10634−10640.
(38) Hou, Y. H.; Cai, K. Y.; Li, J. H.; Chen, X. Y.; Lai, M.; Hu, Y.; Luo, Z. W.; Ding, X. W.; Xu, D. W. Effects of titanium nanoparticles on adhesion, migration, proliferation, and differentiation of mesenchymal stem cells. *Int. J. Nanomed.* **2013**, *8*, 3619−3630.
(39) Huang, X.; Teng, X.; Chen, D.; Tang, F.; He, J. The effect of the shape of mesoporous silica nanoparticles on cellular uptake and cell function. *Biomaterials* **2010**, *31* (3), 438−448.

(40) Yuan, Y.; Liu, C.; Qian, J.; Wang, J.; Zhang, Y. Size-mediated cytotoxicity and apoptosis of hydroxyapatite nanoparticles in human hepatoma HepG2 cells. *Biomaterials* **2010**, *31* (4), 730−40.
(41) Yin, M.; Yin, Y.; Han, Y.; Dai, H.; Li, S. Effects of uptake of hydroxyapatite nanoparticles into hepatoma cells on cell adhesion and proliferation. *J. Nanomater.* **2014**, *2014*, No. 731897.
(42) Chithrani, B. D.; Ghazani, A. A.; Chan, W. C. W. Determining the size and shape dependence of gold nanoparticle uptake into mammalian cells. *Nano Lett.* **2006**, *6* (4), 662−668.
(43) Rao, C. Y.; Sun, X. Y.; Ouyang, J. M. Effects of physical properties of nano-sized hydroxyapatite crystals on cellular toxicity in renal epithelial cells. *Mater. Sci. Eng., C* **2019**, *103*, No. 109807.

https://doi.org/10.1021/acsomega.3c08180
ACS Omega 2023, 8, 48432−48443